Archives of Toxicology (2019) 93:3305–3320
https://doi.org/10.1007/s00204-019-02572-w

ORGAN TOXICITY AND MECHANISMS

Aflatoxin B1 enhances pyroptosis of hepatocytes and activation of Kupffer cells to promote liver inflammatory injury via dephosphorylation of cyclooxygenase-2: an in vitro, ex vivo and in vivo study

Li-Yin Zhang[1] · Deng-Lin Zhan[1] · Yuan-Yuan Chen[1] · Wei-Hua Wang[1] · Cheng-Yong He[1] · Yi Lin[1] · Yu-Chun Lin[1] · Zhong-Ning Lin[1]

Received: 23 April 2019 / Accepted: 17 September 2019 / Published online: 14 October 2019

Abstract

Aflatoxin B1 (AFB1), a food contaminant derived from Aspergillus fungi, has been reported to cause hepatic immunotoxicity via inflammatory infiltration and cytokines release. As a pro-inflammatory factor, cyclooxygenase-2 (COX-2) is widely involved in liver inflammation induced by xenobiotics. However, the mechanism by which AFB1-induced COX-2 regulates liver inflammatory injury via hepatocytes-Kupffer cells (KCs) crosstalk remains unclear and requires further elucidation. Here, we established a COX-2 upregulated model with AFB1 treatment in vivo (C57BL/6 mice, 1 mg/kg body weight, i.g, 4 weeks) and in vitro (human liver HepaRG cells, 1 μM for 24 h). In vivo, AFB1-treated mice exhibited NLRP3 inflammasome activation, inflammatory infiltration, and increased recruitment of KCs. In vitro, dephosphorylated COX-2 by protein phosphatase 2A (PP2A)-B55δ promoted NLRP3 inflammasome activation, including mitochondrial translocation of NLRP3, caspase 1 cleavage, and IL-1β release. Moreover, phosphorylated COX-2 at serine 601 (p-COX-2^{Ser601}) underwent endoplasmic reticulum (ER) retention for proteasome degradation. Furthermore, pyroptosis and inflammatory response induced by AFB1 were relieved with COX-2 genetic (si*PTGS2*) intervention or pharmaceutic (celecoxib, 30 mg/kg body weight, i.g, 4 weeks) inhibition of COX-2 via NLRP3 inflammasome suppression in vivo and in vitro. Ex vivo, in a co-culture system with murine primary hepatocytes and KCs, activated KCs induced by damaged signals from pyroptotic hepatocytes, formed a feedback loop to amplify NLRP3-dependent pyroptosis of hepatocytes via pro-inflammatory signaling, leading to liver inflammatory injury. Taken together, our data suggest a novel mechanism that protein quality control of COX-2 determines the intracellular distribution and activation of NLRP3 inflammasome, which promotes liver inflammatory injury via hepatocytes-KCs crosstalk.

Keywords Aflatoxin B1 · Cyclooxygenase-2 · NLRP3 inflammasome · Protein phosphatase 2A · Kupffer cells · Liver inflammatory injury

Introduction

Chronic liver inflammation drives hepatic fibrosis and cirrhosis, which accounts for more than 1 million deaths per year worldwide (Mokdad et al. 2014). Liver inflammatory injury is closely related to xenobiotics exposure, which was involved in multiple liver diseases, including viral hepatitis, alcoholic liver disease (ALD), and nonalcoholic steatohepatitis (NASH) (Koyama and Brenner 2017). Aflatoxin B1 (AFB1), a carcinogenic mycotoxin widely found in mildewed cereals, targets liver tissue through gastrointestinal route (Rushing and Selim 2019). Studies have shown

Li-Yin Zhang and Deng-Lin Zhan contributed equally to this work.

Electronic supplementary material The online version of this article (https://doi.org/10.1007/s00204-019-02572-w) contains supplementary material, which is available to authorized users.

✉ Yu-Chun Lin
linych@xmu.edu.cn

✉ Zhong-Ning Lin
linzhn@xmu.edu.cn

[1] State Key Laboratory of Molecular Vaccinology and Molecular Diagnostics, School of Public Health, Xiamen University, Xiang'an South Road, Xiamen 361102, China

that hepatic regional microenvironment, regulated by pro-inflammatory cytokines induced by AFB1, promoted liver inflammatory injury. The secretion of IL-1β in rat serum was increased by AFB1, accompanied by hepatic hemorrhage and inflammatory infiltration (Akinrinmade et al. 2016). The expression of cyclooxygenase-2 (COX-2) and interleukin-6 (IL-6) were upregulated via activating nuclear factor-κB (NF-κB) signaling pathway in liver tissue of zebrafish with AFB1 treatment (Lu et al. 2013). Hepatic cytochrome P450 (CYP450) was required during the metabolic process from AFB1 to its toxic metabolite 8,9-epoxide (AFBO), indicating hepatocyte damage was the main reason for the hepatotoxicity of AFB1 (Ueng et al. 1995). However, due to the characteristic of the sinusoidal structure of hepatic regional immunity, liver inflammatory injury depends on the composition and activity of hepatic immune cells and the crosstalk with hepatocytes (Byun and Yi 2017). It is necessary to further determine the potential mechanism of the crosstalk between hepatocytes and hepatic immune cells during AFB1 exposure.

Pyroptosis, a mode of programmed cell death marked by a ruptured plasma membrane, is recently thought to be an immunogenic process via releasing damage-associated molecular patterns (DAMPs) (Garg et al. 2015; Zhang et al. 2018). Of the defined inflammasomes, NOD-like receptor protein 3 (NLRP3) inflammasome is well studied in response to endogenous or exogenous dangerous signals. NLRP3 inflammasome is a multi-protein complex with the adaptor, apoptosis-associated speck-like protein containing a caspase recruitment domain (ASC) (Lamkanfi and Dixit 2014). NLRP3 inflammasome functions as a molecular platform for the activation of cysteine protease caspase 1, leading to maturation and secretion of pro-interleukin-1β (pro-IL-1β) and pro-interleukin-18 (pro-IL-18). Meanwhile, active caspase 1 cleaves gasdermin D (GSDMD) to form pores on cellular plasma membrane (Sarhan et al. 2018). Previous studies used to focus on the functional analysis of NLRP3 inflammasome in liver resident Kupffer cells (KCs) which account for 80–90% of tissue macrophages of the whole body (Li et al. 2017; Mridha et al. 2017). However, whether NLRP3 inflammasome-related pyroptosis mediates hepatocytes-KCs crosstalk remains to be elucidated.

COX-2, a rate-limiting enzyme catalyzing arachidonic acid to prostaglandins (PGs), is an endoplasmic reticulum (ER)-resident protein widely involved in regional inflammatory responses induced by xenobiotics or pro-inflammatory cytokines (Alexanian and Sorokin 2017). Inhibition of COX-2 by pharmaceutic (SC-791) or genetic knockdown reduced lipopolysaccharide (LPS)-induced NLRP3 inflammasome activation of murine macrophage J774A.1 cells by decreasing synthesis of PGs and lessening mitochondrial oxidative damage (Hua et al. 2015). Although studies have demonstrated the correlation between COX-2 and NLRP3 inflammasome, the mechanism of NLRP3 inflammasome activation regulated by COX-2 in liver inflammatory injury remains to be elucidated. Interestingly, COX-2 contains a phosphorylated motif which can be activated by protein tyrosine phosphatase (PTP) in cerebral endothelial cells (Alexanian and Sorokin 2017). Therefore, the mechanism of the phosphorylation status of COX-2 on its intracellular distribution and function has attracted our attention. Protein phosphatase 2A (PP2A), a serine/threonine phosphatase, is related to cell signaling and hepatotoxicity induced by xenobiotics. Because of the diversity of B subunits in the holoenzyme trimer, PP2A has substrate-specificity and targeted-selectivity (Reynhout and Janssens 2018). Whether NLRP3 inflammasome activation is regulated by dephosphorylation of COX-2 modified by PP2A remains to be studied. In the present study, we establish a COX-2 upregulated model with AFB1 in vivo and in vitro. We for the first time reveal that protein quality control (PQC) of COX-2, PP2A-B55δ-mediated dephosphorylation of COX-2^{Ser601} induced by AFB1, altered ER localization of COX-2 and promoted recruitment and activation of NLRP3 inflammasome in hepatocytes. Moreover, a positive feedback loop from activated KCs to hepatocytes stimulated immune cascade and amplified liver inflammatory injury.

Materials and methods

Gene expression omnibus (GEO) database analysis

The mRNA expression dataset GSE25844 was obtained from the GEO database (http://www.ncbi.nlm.nih.gov/geo/). Three independent biological replicates of HepaRG cells were stimulated with AFB1 (0.05, 0.25 μM) for 24 h. The relative expression of indicated genes in AFB1-treated group was compared with the control group. And the correlations between relative expression of indicated genes were analyzed by Pearson's correlation regression analysis.

In vivo experimentation

C57BL/6 mice (15–25 g) were randomly divided into groups as follows: control (corn oil), celecoxib (CELE, MedChemExpress, NJ, USA) treated (30 mg/kg, i.g, CELE group), AFB1 (Fermentek, Israel) treated (1 mg/kg, i.g, AFB1 group), and AFB1 with combined treatment of CELE (AFB1 + CELE group) ($n = 12$ in each group). CELE or AFB1 was dissolved in corn oil in a volume less than 200 μL. The mice were intragastrically administered every other day for 4 weeks. All mice were sacrificed for experimental purposes after 24 h from the last exposure. Animal Ethical Committee of Xiamen University approved all the animal

experiments which were conducted in accordance with the guidelines of the National Institutes of Health (NIH).

Ex vivo experimentation

Primary hepatocytes The previously described improved method of "the in situ two-step collagenase perfusion to heart-based perfusion" was followed (Li et al. 2010). In brief, after 8 h fasting, mice were anesthetized and fixed on the anatomical board. Apex cordis and liver were exposed to insert needle at ventriculus sinister. The perfusion was conducted sequentially with calcium-free solution (NaCl 8.3 g/L, KCl 0.5 g/L, HEPES 2.4 g/L, EGTA 0.38 g/L, pH 7.4) and collagenase solution (NaCl 3.9 g/L, KCl 0.5 g/L, HEPES 2.4 g/L, $CaCl_2$ 0.55 g/L, pH 7.6) containing collagenase IV (Solabio, Beijing, China) until liver couldn't rebound after pressing. The perfusion solutions were preheated at 37 °C and the flow rate was 60 r/min. Liver was completely detached from the digestion with collagenase IV, DNases (Solabio) and proteinase K (Merck, Germany), for 5–10 min at 37 °C. The liver capsule was torn off to obtain cell suspension and centrifuged at 50×*g* for 3 min for 3 times after passing through a 200-mesh filter. About 5×10^5 cells per well were seeded into a 6-well plate after counting, and the medium was replaced after cell adherence about 4 h.

Primary KCs Liver was extracted by anatomical separation after execution, and digested by mouse Liver Dissociation Kit (Miltenyi Biotec, Germany) using gentleMACS™ Dissociators (Miltenyi Biotec) to obtain cell suspension. KCs were sorted by MACS magnetic microbeads coated with anti-F4/80 antibody and MACS columns (Miltenyi Biotec), according to KCs' surface marker expression. About 2.5×10^5 KCs per well were seeded into the lower or upper chamber of transwell (Corning, NY, USA) for co-culture with primary hepatocytes after elution, and the medium was replaced after cell adherence about 2 h.

Primary cells were cultured in Williams' Medium E with GlutaMAX-I (Gibco, CA, USA) supplemented with 10% fetal bovine serum (FBS) (Gibco), 1% (v/v) penicillin-streptomycin (Life, NY, USA), 4 μg/mL of bovine insulin (Wanbang, Jiangsu, China), and 5×10^{-5} mol/L of hydrocortisone hemisuccinate (Sigma, MO, USA).

In vitro experimentation

HepaRG cells were obtained from the National Institute of Diagnostics and Vaccine Development in Infectious Diseases (Xiamen University). Cell culture and differentiation for HepaRG cells were described in our previous study (He et al. 2018). Human normal hepatic cell line L02 and human embryonic kidney cell line HEK-293T were maintained in our laboratory, cultured in RPMI 1640 medium (Hyclone, UT, USA) and in Dulbecco's Modified Eagle Medium (DMEM) high glucose medium (Hyclone) which was supplemented with 10% FBS and 1% (v/v) penicillin-streptomycin, respectively. All cells were maintained at 37 °C in a humidified atmosphere of 5% CO_2.

Site-directed mutagenesis

High-fidelity KOD-Plus enzyme was performed by inverse PCR with KOD-Plus Mutagenesis Kit (Toyobo, Japan). As a DNA template, pB-*PTGS2*-Flag was completely amplified with two primers in the opposite direction, to generate base mutation from serine to alanine (S to A) or to aspartate (S to D) at serine 582, 583, 584, 586, and 601 of COX-2. Then, the PCR products were self-ligated by T4 polynucleotide kinase. The primers were listed in Table S1 and indicated bases of mutant sites were underlined and bolded. Construction of pB-*PTGS2* and establishment of stable cell lines were as described in our previous study (Liao et al. 2015).

Statistics

Data were expressed as mean ± standard deviation (SD) of at least three independent experiments. Statistical analyses were executed with Statistical Package for Social Sciences (SPSS) version 16.0. Unpaired Student's *t*-test and one-way analysis of variance (ANOVA) were applied for determining the statistical significance. $P < 0.05$ was considered as significant difference.

Results

GEO analysis of pro-inflammatory genes induced by AFB1 in HepaRG cells

In this study, the outcomes of regulatory cell death (RCD) were concerned in hepatocytes induced by AFB1. It is known that members of the caspase family are the most important molecules in various RCD (Julien and Wells 2017; Van Opdenbosch and Lamkanfi 2019). To investigate AFB1-induced liver inflammatory injury and cell death patterns of hepatocytes, the levels of caspase-related genes in AFB1-treated HepaRG cells were analyzed using the GEO dataset (GSE25844). Among caspase-related genes, the relative levels of *CASP1* (encoding gene for caspase 1) and *CASP3* (encoding gene for caspase 3) increased significantly in AFB1-treated HepaRG cells (Fig. 1a). Caspase 1-dependent pyroptosis and caspase 3-dependent apoptosis were regarded as immunogenic cell death, which suggest AFB1 induced liver inflammatory injury via releasing DAMPs from dying hepatocytes. Moreover, the relative level of *PTGS2* (encoding gene for COX-2), a pro-inflammatory gene, was upregulated in AFB1-treated HepaRG cells (Fig. 1b). The relative

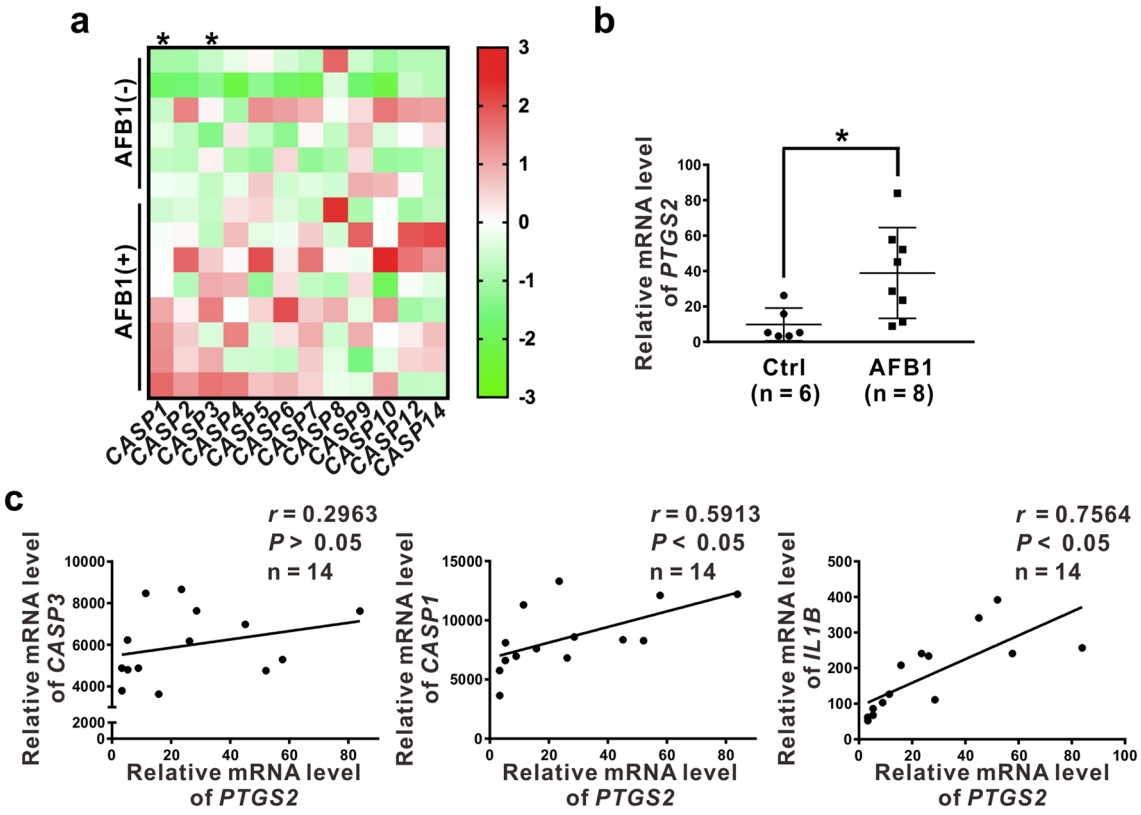

Fig. 1 GEO analysis of pro-inflammatory genes in HepaRG cells induced by AFB1. **a–c** The relative mRNA levels of indicated genes were obtained from NCBI, GEO database (GSE25844). HepaRG cells were stimulated with AFB1 (0.05, 0.25 μM) for 24 h. The heat-map of the relative mRNA levels of caspase family (**a**), the relative mRNA level of *PTGS2* (**b**), and the linear correlation between the relative mRNA levels of *PTGS2* and *CASP3*, *CASP1*, or *IL1B* (**c**) were represented. *$P < 0.05$, compared with control group

level of *PTGS2* was positively correlated with *CASP1* ($r = 0.5913$, $P < 0.05$) or *IL1B* (encoding gene for IL-1β) ($r = 0.7564$, $P < 0.05$), while the correlation of *PTGS2* with *CASP3* was not significant (Fig. 1c). As mentioned before, active caspase 1 determines the rupture of cellular plasma membrane and maturation of IL-1β. These results indicate that liver inflammatory injury induced by AFB1 was closely related to caspase 1-dependent pyroptosis and the expression of COX-2.

Inhibition of COX-2 reversed liver inflammatory injury induced by AFB1 in vivo

Interestingly, consistent with the outcomes observed from GEO analysis, the protein levels of COX-2, p10 (the active form of caspase 1), and IL-1β were upregulated in liver tissues of AFB1-exposed mice in our study (Fig. S1a). To further verify the role of COX-2 in liver inflammatory injury and its relationship with pyroptosis of hepatocytes, we established an exposure model of AFB1 and a CELE intervention model (a selective inhibitor of COX-2) in vivo. The growth curve of AFB1- or CELE-treated group had no significant changes compared to the control group (Fig. S1b). In AFB1-exposed mice, the mRNA levels of hepatic *Cyp1a2* and *Cyp3a11* of CYP450 were upregulated, while *Gsta*, *Gstm*, and *Gstt* of glutathione S-transferase (GSTs) were downregulated (Fig. S1c), indicating the metabolic activation in AFB1-treated group. Moreover, the mRNA level of *Ptgs2* was increased in AFB1-treated group, and decreased in CELE-treated group (Fig. S1c), indicating that the induction of COX-2 in liver tissue could be upregulated by AFB1 and as a target for intervention with CELE. In AFB1-exposed mice, the ratio of liver/body weight was increased (Fig. 2a). Moreover, inflammatory foci, inflammatory infiltration of KCs, cell death, and slight collagen deposition were observed in AFB1-treated group (Fig. 2a), consistent with the enhanced hepatic mRNA level of pro-inflammatory cytokines, *Il1b*, *Il18*, *Il6*, and *Tnfa* (Fig. 2b), indicating that AFB1 promoted a pro-inflammatory micro-environment in liver. And the activities of ALT and AST in liver homogenization were increased (Fig. 2c), but remained unchanged in serum (Fig. S1d), prompting that pro-inflammatory environment induced by AFB1 contributed to liver inflammation and injury. However, the mRNA level of pro-inflammatory cytokines, inflammatory infiltration, and liver injury were reduced in CELE pre-treated AFB1-exposed

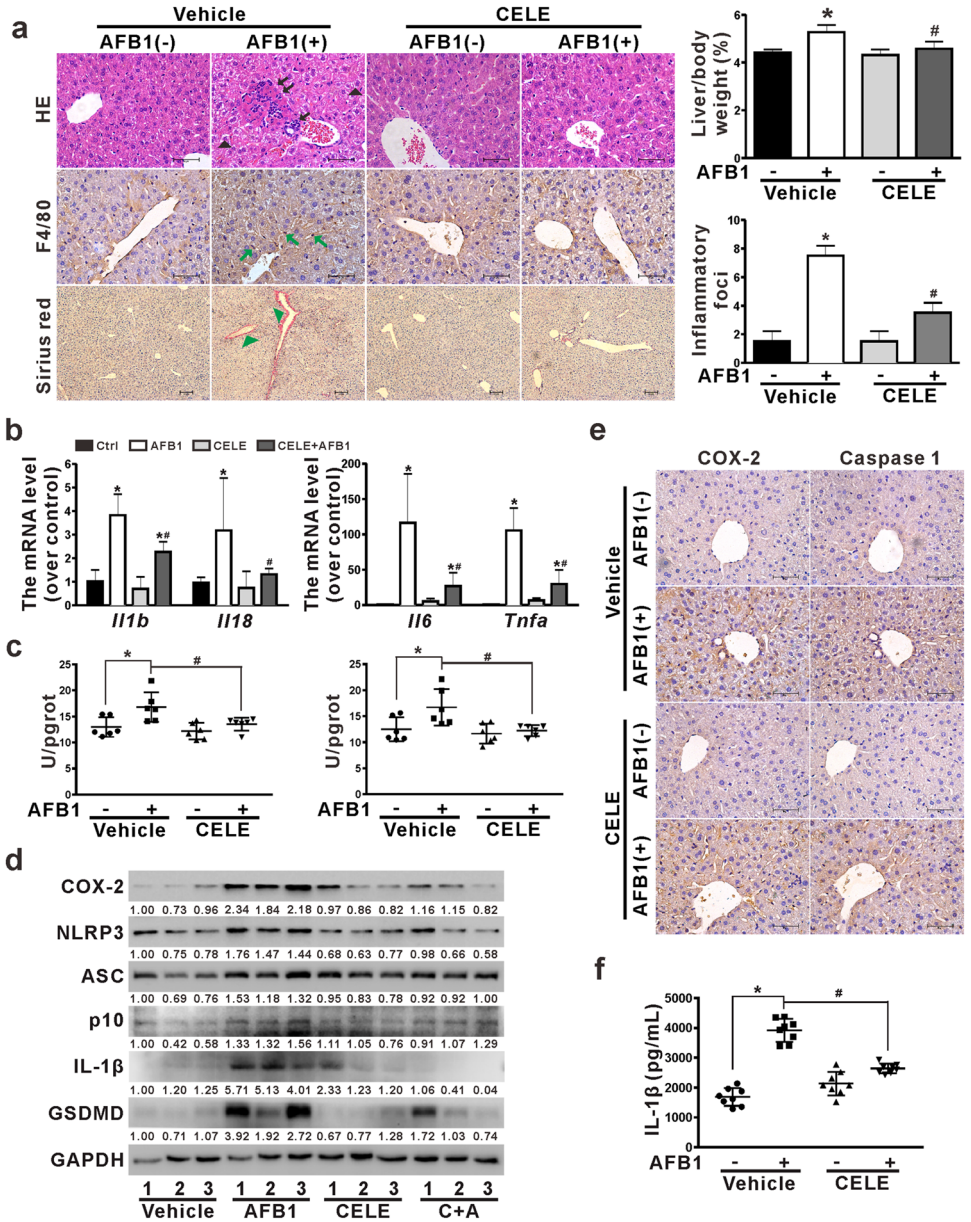

Fig. 2 Inhibition of COX-2 reversed liver inflammatory injury induced by AFB1 in vivo. C57BL/6 mice were treated with AFB1 (1 mg/kg, i.g, AFB1 group) or/and celecoxib (30 mg/kg, i.g, CELE group) for 4 weeks. $n=12$ in each group. **a** Inflammatory foci (black arrow) and cell death (black triangle), collagen deposition (green triangle), inflammatory infiltration of KCs (green arrow) were detected by hematoxylin and eosin (HE) staining, Sirius red staining and IHC analysis of anti-F4/80 antibody (left panel). Scale bar 50 μm or 100 μm. Quantification of inflammatory foci was shown in the bar chart (right panel). Liver/body weight ratio was shown in the bar graph. **b** Hepatic mRNA expression of pro-inflammatory cytokines, *Il-1b*, *Il-18*, *Il-6*, and *Tnf-a*, was detected by qRT-PCR. **c** Activities of ALT (left) and AST (right) in liver homogenate indicated liver injury were measured. **d** The expression of COX-2 and NLRP3 inflammasome-related proteins was examined by western blot (WB). **e** Serial sections were used for IHC analysis for the expression of COX-2 and caspase 1. **f** IL-1β level of liver homogenate was quantified by enzyme-linked immunosorbent assay (ELISA). GAPDH or *ACTB* was served as a loading control for WB and qRT-PCR analysis. Representative examples were displayed. All data were shown as mean ± SD ($n=3$). $^{*}P<0.05$, compared with control group. $^{\#}P<0.05$, compared with AFB1 treated group (colour figure online)

mice, indicating that targeted intervention of COX-2 selectively inhibited the pro-inflammatory environment and liver inflammatory injury induced by AFB1. Furthermore, the levels of proteins representing assembly (NLRP3, ASC, and p10) and activation (IL-1β and GSDMD) of NLRP3 inflammasome in liver tissues were enhanced in AFB1-exposed mice (Fig. 2d). Moreover, the assembly and activation of NLRP3 inflammasome were reduced in CELE group, indicating that CELE intervention was useful for the inhibition of liver inflammation. Furthermore, in AFB1-exposed

mice, the expressions of COX-2 and caspase 1 at the same location were upregulated, determined using immunohistochemical (IHC) analysis (Fig. 2e). A decreased expression of caspase 1 was observed, consistent with reduced COX-2 in CELE-treated group. In addition, IL-1β secretion in serum and liver homogenate was increased in AFB1-treated group, but reduced in CELE-treated group (Fig. S1e; Fig. 2f), indicating that AFB1 induced liver regional inflammation via NLRP3 inflammasome activation and the process mediated by the induced COX-2. In short, these results suggest that AFB1 induced NLRP3-dependent pyroptosis of hepatic cells via upregulated COX-2. DAMPs and IL-1β released from the pyroptotic hepatocytes promoted a series of pro-inflammatory responses to form a hepatic regional immune microenvironment and induce liver inflammation. The selective inhibition of COX-2 could alleviate pyroptotic cell death, pro-inflammatory response, and liver inflammatory injury.

Kupffer cells enhanced NLRP3 inflammasome activation of hepatocytes through inflammatory signaling

To investigate whether the hepatic immune microenvironment was mediated by NLRP3 inflammasome-dependent pyroptosis and was via the crosstalk between hepatocytes and hepatic regional immune cells, the specific subsets of immune cells were analyzed by flow cytometry ex vivo. The ratio of hepatic monocytes, marked by CD11c, had no significant changes in AFB1-treated group (Fig. S1f). The subset of hepatic resident macrophage, namely KCs marked by F4/80, is a source of pro-inflammatory cytokines. It was found that the proportion of F4/80-positive KCs in liver non-parenchymal cells was augmented in AFB1-treated group (16.57%), and was inhibited in CELE-treated group (5.71%) (Fig. 3a). These results indicate that KCs might play an important role in activating immune cascades of hepatic local immunity to aggravate liver regional inflammation.

To further explore the mechanism of activated KCs-mediated regional immune cascades for liver inflammatory injury, primary KCs and hepatocytes were obtained to establish a co-culture model ex vivo. In primary KCs, the nuclear translocation of NF-κB (p65), activator protein-1 (AP-1), and c-JUN were increased, accompanied with the enhanced expression of signal transducer and activator of transcription 3 (STAT3) in AFB1-treat group (Fig. 3b). This indicated that KCs were activated via nuclear transcriptional-dependent pro-inflammatory signaling. Except for enhanced expression of NLRP3 and pro-IL-1β regulated by NF-κB in primary KCs in AFB1-treat group (Fig. 3b), the levels of COX-2, and proteins representing assembly (NLRP3, ASC, and p10) and activation (IL-1β and GSDMD) of NLRP3 inflammasome were upregulated in primary hepatocytes (Fig. 3c). Moreover, IL-1β secretion in the supernatant of both primary hepatocytes and KCs were increased in AFB1-treated group and decreased after COX-2 intervention in CELE-treated group (Fig. 3d). These results indicate that AFB1 induced NLRP3 inflammasome-dependent pyroptosis via upregulated COX-2 in both hepatocytes and KCs. Furthermore, in a co-culture system of primary hepatocytes and KCs from the control group, with the administration of AFB1 after cell adherence, the protein levels of COX-2, NLRP3, ASC, p10, IL-1β, and GSDMD in primary hepatocytes were upregulated, consistent with the increased IL-1β secretion in the supernatant (Fig. 3e). And in the co-culture system of primary hepatocytes and KCs from AFB1-treated group, primary hepatocytes were treated with CY-09 after adherence, an inhibitor of NLRP3 synthesized previously (Jiang et al. 2017). The protein levels described above in primary hepatocytes were downregulated, consistent with the reduced IL-1β secretion in the supernatant (Fig. S1g).

To elucidate the crosstalk between KCs and hepatocytes in liver inflammatory injury, primary hepatocytes and KCs were obtained from un-treated C57BL/6 mice and re-seeded into monolayer or transwell chamber for co-culture, with additional AFB1 treatment after cell adherence. Compared to hepatocytes of monolayer-culture, the protein levels of COX-2, NLRP3, ASC, p10, IL-1β, and GSDMD were significantly upregulated in hepatocytes of co-culture with KCs (Fig. 3f), indicating that KCs formed a feedback loop to hepatocytes via aggravating NLRP3 inflammasome activation. In general, AFB1 induced NLRP3-dependent pyroptosis of hepatocytes to augment pro-inflammatory signaling of KCs and the activated KCs aggravated NLRP3 inflammasome activation of hepatocytes, which formed a vice cycle to enhance liver inflammatory injury.

AFB1 induced NLRP3 inflammasome activation and plasma membrane rupture in HepaRG cells

With the GEO dataset (GSE87028), analysis for other members of the NLR family were performed. The relative expression levels of NLR family members in HepaRG cells with AFB1 treatment were shown in figures S2a and S2b. Indeed, the relative levels of *NLRP1* and *NLRP3* were significantly upregulated (Fig. S2a). Furthermore, the relative levels of *PTGS2* and *NLRP3* were positively correlated in AFB1-treated HepaRG cells (Fig. S2b). With our experiments, the transcription of NLR families' genes (including *NLRP1*, *NLRP2*, *NLRP3*, and *NLRC4*) was examined in HepaRG cells exposed to AFB1, while the mRNA level of *NLRP3* gene was significantly increased (Fig. S2c).

To further verify the mechanism of pyroptosis induced by AFB1 in vitro, the differentiated HepaRG cells were treated with 1 μM AFB1 for 24 h. And the metabolic activity of differentiated cells was verified by the expression of hepatic *CYP1A1*, *2B6*, *3A4*, and *7A1* (Fig. S2d). The features of

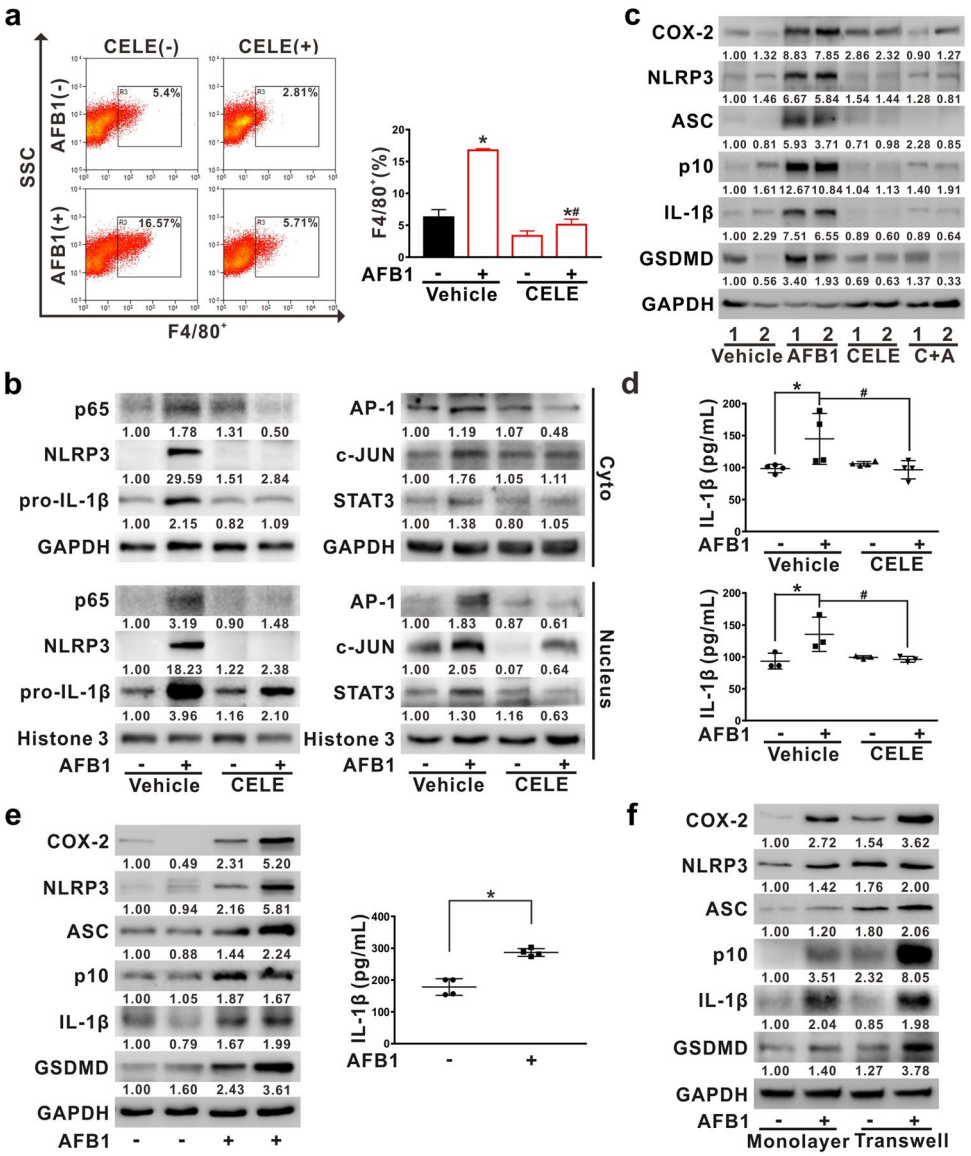

Fig. 3 Kupffer cells enhanced NLRP3 inflammasome activation of hepatocytes through inflammatory signaling. Primary hepatocytes and KCs were obtained by heart-liver perfusion and magnetic beads, respectively. **a** The proportion of F4/80-positive cells (indicated KCs) of hepatic non-parenchymal cells was detected by flow cytometry analysis after digestion of the liver (left panel). Quantification of fluorescence intensity was shown in the bar chart (right panel). **b** The protein levels of NF-κB (p65), AP-1, c-JUN, and STAT3 in cytosolic (Cyto) or nuclear (Nucleus) fraction of primary KCs were detected by WB. **c** The expression of COX-2 and NLRP3 inflammasome-related protein of primary hepatocytes were examined by WB. **d** IL-1β secretion in the supernatants from primary KCs (upper panel) and hepatocytes (lower panel) were quantified by ELISA. **e** Primary hepatocytes and KCs from corn oil-treated control group were obtained and re-seeded in the lower and upper chamber of transwell for 48 h, respectively. And primary hepatocytes were treated with AFB1 (1 μM, 24 h). Proteins representing NLRP3 inflammasome activation and COX-2 were detected by WB, and IL-1β secretion in the supernatant was quantified by ELISA. **f** Primary hepatocytes were obtained from non-treated C57BL/6 mice, and re-seeded into monolayer or lower chamber of the transwell. For co-culture, primary KCs from non-treated C57BL/6 mice were re-seeded into the upper chamber of the transwell. Indicated protein levels of primary hepatocytes from monolayer- or transwell-culture were detected by WB. GAPDH served as a loading control for WB analysis. Representative examples were displayed. All data were shown as mean ± SD ($n = 3$). *$P < 0.05$, compared with control group. #$P < 0.05$, compared with AFB1 treated group

pyroptosis, including pyroptosis bodies of early phase and membrane rupture of terminal phase, were observed using transmission electron microscope (TEM) (Fig. 4a). With immunofluorescence (IF) analysis, cytoplasmic expansion and increased fluorescent signal of GSDMD were observed (Fig. 4b). These data indicate pyroptosis was induced in HepaRG cells with AFB1 treatment. Then, we further studied whether pyroptosis of hepatocytes is NLRP3

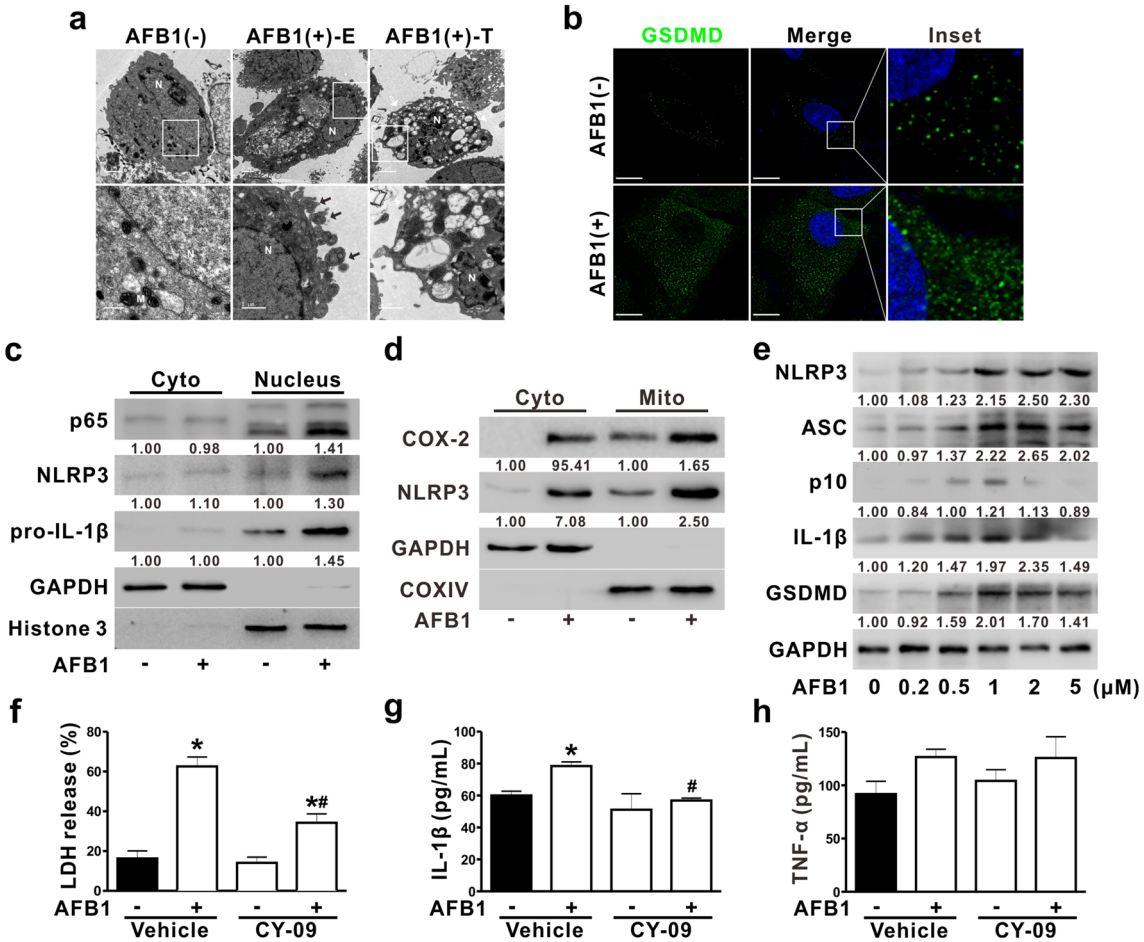

Fig. 4 AFB1 induced NLRP3 inflammasome activation and plasma membrane rupture in HepaRG cells. Differentiated HepaRG cells were treated with AFB1 (1 μM, 24 h). **a** Pyroptosis bodies (black arrows) and membrane rupture (white arrows) were observed by a transmission electron microscope. *E* early phase, *T* terminal phase, *N* nucleus, *M* mitochondrion. Scale bar 2 μm or 1 μm. **b** Cells were subjected to IF staining of anti-GSDMD (green) and detected by confocal microscopy. ER-Tracker staining (red) represented the ER, and DAPI staining (blue) represented the nucleus. Scale bar 10 μm. **c** The protein levels of NF-κB (p65), NLRP3, and pro-IL-1β from cytoplasmic (Cyto) or nuclear (Nucleus) fractions were determined by WB. **d** The protein levels of NLRP3 and COX-2 from cytoplasmic (Cyto) or mitochondrial (Mito) fractions were detected by WB. **(e)** Proteins representing the assembly (NLRP3, ASC, and p10) and activation (IL-1β and GSDMD) of NLRP3 inflammasome were determined by WB, treated with the indicated concentration of AFB1 for 24 h. **f–h** Cells were co-treated with CY-09 (1 μM, 24 h) and AFB1 (1 μM, 24 h) or not. Plasma membrane rupture was analyzed by LDH release assay (**f**). IL-1β and TNF-α secretion in the supernatants was quantified by ELISA (**g, h**). GAPDH, Histone 3, and COXIV were served as the loading control of Cyto, Nucleus, and Mito fractions, respectively. Representative examples were displayed. All data were shown as mean ± SD. $^{*}P < 0.05$, compared with control group. $^{\#}P < 0.05$, compared with AFB1 treated group (colour figure online)

inflammasome dependent. Nuclear translocation of NF-κB (p65), expression of NLRP3, and pro-IL-1β were enhanced (Fig. 4c). Meanwhile, increased mitochondrial translocation of NLRP3 and its co-localization with ASC suggest that the recruitment and assembly activation of NLRP3 were dependent on mitochondria and essential for caspase 1 activity (Fig. 4d; Fig. S2e, S2f). The proteins representing downstream of caspase 1 activation, including p10, IL-1β, and GSDMD were also upregulated (Fig. 4e). Consistent with observed membrane rupture, lactate dehydrogenase (LDH) leakage and IL-1β release were significantly increased (Fig. 4f, g), which could be relieved by CY-09. However, changes in TNF-α release in the supernatant were not observed (Fig. 4h). In brief, these results indicate that the NLRP3 inflammasome activation and the membrane rupture induced by AFB1 lead to pyroptosis of hepatocytes.

NLRP3 inflammasome activation was regulated via AFB1-induced COX-2 upregulation

Consistent with the upregulation of COX-2 induced by AFB1 in liver tissue or primary hepatocytes in vivo or ex vivo model, the level of *PTGS2* mRNA and COX-2 protein were upregulated in AFB1-treated HepaRG cells (Fig.

S2g). Moreover, mitochondrial translocation of COX-2 was observed as that of NLRP3, which indicate that COX-2 was localized closely with NLRP3 on mitochondria (Fig. 4d). To further investigate the role of COX-2 in the activation of the NLRP3 inflammasome, we used small interfering RNA (siRNA) for *PTGS2* (si*PTGS2*) to suppress the expression of COX-2. Compared to AFB1-treated siRNA negative control (siNC) cells, the fluorescence intensity of COX-2 and co-localization between NLRP3 and MitoTracker were decreased in AFB1-treated si*PTGS2* cells, indicating that COX-2 intervention reduced the mitochondria translocation of NLRP3 (Fig. 5a). Proteins representing assembly (NLRP3, ASC, and p10) and activation (IL-1β and GSDMD) of NLRP3 inflammasome were reduced after COX-2 intervention (Fig. 5b), accompanied by the decreased LDH leakage and IL-1β release (Fig. 5c, d). These results suggest that COX-2 regulated the mitochondrial recruitment and activation of the NLRP3 inflammasome, which might contribute to pyroptosis for DAMPs and IL-1β release.

Dephosphorylation of COX-2 by PP2A-B55δ regulated NLRP3 inflammasome activation

It has been demonstrated that COX-2 contained a phosphorylated motif, which was crucial for its activity and function (Alexanian and Sorokin 2017). To investigate the contribution of the phosphorylated status of COX-2 on NLRP3 inflammasome activation, we established a series of cell lines expressing phosphorylation (aspartate mutation from serine) or dephosphorylation (alanine mutation from serine) of COX-2. As predicted with the PhosphoNET and DISPHOS previously, serine 582, 583, 584, 586, and 601 were the possible phosphorylated sites at C-terminus of COX-2 (Fig. S3a, S3b). These five serine (S) sites were mutant to alanine (A) or aspartate (D) respectively, representing dephosphorylated or phosphorylated COX-2, as shown in the schematic view (Fig. 6a). Compared with L02-pBabe cells (wild type control), the increased expression of NLRP3 and ASC were observed in COX-2^{S601A} cells (with dephosphorylated COX-2), consistent with upregulated IL-1β and GSDMD through caspase 1 cleavage (Fig. 6b). Moreover,

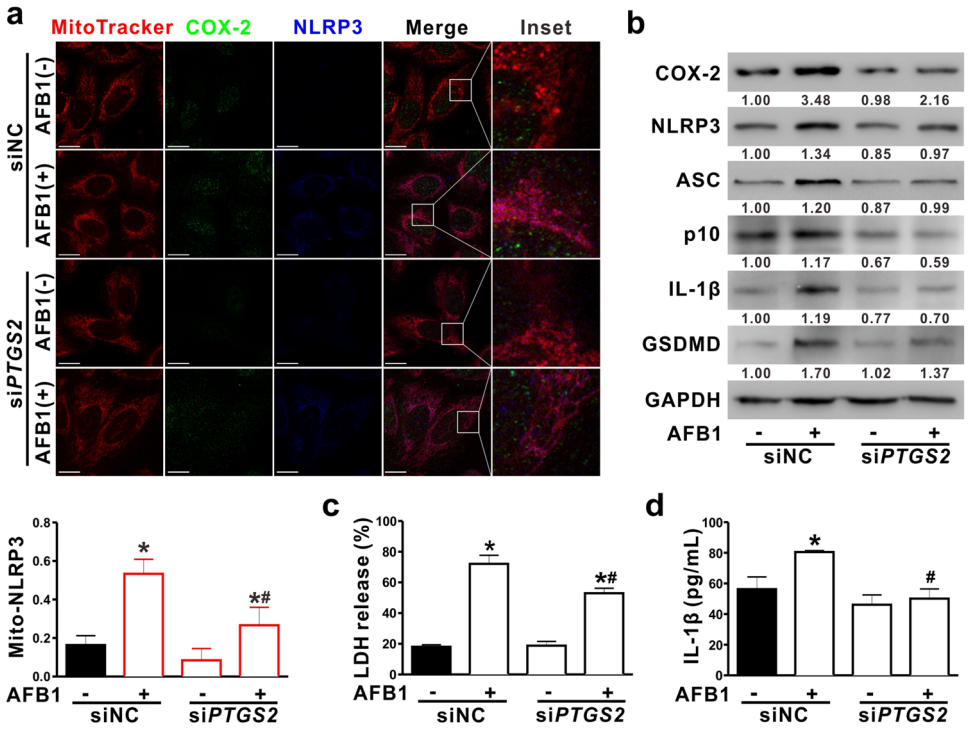

Fig. 5 NLRP3 inflammasome activation was regulated via upregulated COX-2 induced by AFB1. Differentiated HepaRG cells were transfected with siNC or si*PTGS2* (50 nM) for 6 h, followed by AFB1 treatment (1 μM 24 h). **a** The expression of COX-2 (green) and NLRP3 (blue), and co-localization of MitoTracker (red) and NLRP3 were examined by confocal microscopy (upper panel). Scale bar 10 μm. And Pearson's correlation for the co-localization of mitochondria with NLRP3 was shown in the bar graph (lower panel). The overlap sections of mitochondria and NLRP3 were quantified using ImagePro-plus 6.0. **b** The levels of COX-2 and NLRP3 inflammasome-related proteins were examined by WB. **c** Plasma membrane rupture was analyzed by LDH release assay. **d** IL-1β secretion in the supernatants was quantified by ELISA. GAPDH served as a loading control for WB analysis. Representative examples were displayed. All data were shown as mean ± SD. $^{*}P < 0.05$, compared with siNC control group. $^{\#}P < 0.05$, compared with siNC and AFB1-treated group (colour figure online)

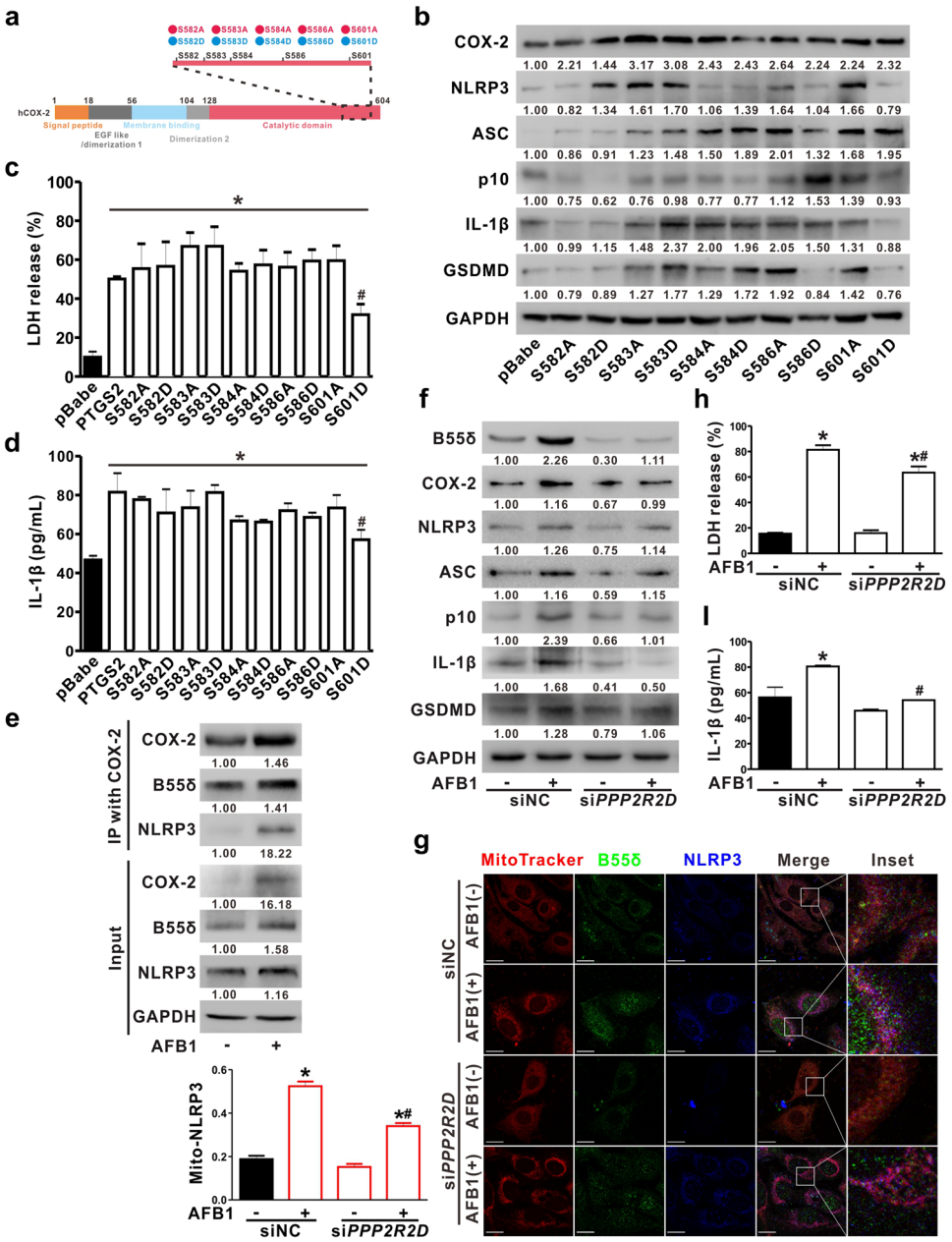

Fig. 6 Dephosphorylation of COX-2 by PP2A-B55δ regulated NLRP3 inflammasome activation. **a** The schematic view of C-terminal site-specific mutagenesis of COX-2. Serine 582, 583, 584, 586, and 601 were mutated to alanine (S to A) for mimicking dephosphorylation or aspartate (S to D) for mimicking phosphorylation of COX-2. **b–d** In L02-pB cells, L02-*PTGS2* cells, or mimic phosphorylated/dephosphorylated COX-2 cells at indicated sites, the expression of NLRP3 inflammasome-related proteins were examined by WB (**b**). Plasma membrane rupture was analyzed by LDH release assay (**c**), and IL-1β secretion in the supernatants was quantified by ELISA (**d**). **e** After treatment of AFB1 (1 μM, 24 h), cell lysates were immunoprecipitated with anti-COX-2 antibody, and both IP and total lysates (Input) were immunoblotted for COX-2, B55δ, and NLRP3. **f–i** Differentiated HepaRG cells were transfected with siNC or si*PPP2R2D* (50 nM) for 6 h, followed by AFB1 treatment (1 μM 24 h). The expression of B55δ, COX-2, and NLRP3 inflammasome-related protein were examined by WB (**f**). The expression of B55δ (green) and NLRP3 (blue), and co-localization of MitoTracker (red) and NLRP3 was examined by confocal microscopy (right panel). Scale bar 10 μm. Pearson's correlation for the co-localization of mitochondria with NLRP3 was shown in the bar graph (left panel). The overlap sections of mitochondria and NLRP3 were quantified using ImagePro-plus 6.0 (**g**). Plasma membrane rupture was analyzed by LDH release assay (**h**), and IL-1β secretion in the supernatants was quantified by ELISA (**i**). GAPDH served as a loading control for WB analysis. Representative examples were displayed. All data were shown as mean ± SD. $^{*}P < 0.05$, compared with L02-pB cell or siNC control group. $^{\#}P < 0.05$, compared with L02-*PTGS2* cell or siNC and AFB1-treated group (colour figure online)

compared to COX-2^{S601A} cells, proteins representing assembly (NLRP3, ASC, and p10) and activation (IL-1β and GSDMD) of NLRP3 inflammasome were decreased in COX-2^{S601D} cells (with phosphorylated COX-2) (Fig. 6b). However, cells harboring other mutant sites had no significant alteration between dephosphorylated and phosphorylated form of COX-2. These results indicate that the phosphorylated status of COX-2^{Ser601} mediated the function of COX-2 for NLRP3 inflammasome activation. Meanwhile, LDH leakage and IL-1β release were significantly increased in dephosphorylated or phosphorylated COX-2-overexpressing cells (Fig. 6c, d). Moreover, the LDH leakage and IL-1β release in COX-2^{S601D} cells were significantly reduced compared to COX-2^{S601A} cells. These results demonstrate that regulatory phosphorylated status of COX-2^{Ser601} as a potential functional site was important for its activity, and dephosphorylated regulation of COX-2^{Ser601} played a role in NLRP3 inflammasome activation.

Protein phosphatases (PPs), including the protein phosphatase 1 (PP1) and PP2 families in mammals, are known to regulate the dephosphorylation of different protein substrates (Bertran et al. 2019; Virshup and Shenolikar 2009). PP2A, a serine/threonine phosphatase, functions as a complex containing catalytic C, scaffold A, and regulatory B subunit family (Alvarez-Fernandez et al. 2018). The substrate targeting and specificity of PP2A are determined by its multifarious B subunits (Reynhout and Janssens 2018). With the GEO dataset (GSE25844), the relative expression levels of *PPP1CA* (encoding gene for PP1Cα catalytic subunit in PP1 family) and *PPP2R2D* (encoding gene for B55δ subunit in PP2A family) were significantly increased in AFB1-treated HepaRG cells (Fig. S3c, S3d). With our experiments, the mRNA levels of *PPP1CA, PPP2R2A*, and *PPP2R2D* were increased in AFB1-induced pyroptosis model of HepaRG cells (Fig. S3e). Furthermore, the positive correlation between the relative expression level of *PPP2R2D* and *PTGS2*, *CASP1*, or *GSDMD* ($r = 0.6680$, 0.5591, 0.5908, $P < 0.05$) was shown (Fig. S3f). In AFB1-exposed mice, the expression of B55δ was upregulated at the same location with COX-2 on serial sections by IHC analysis (Fig. S3g). Moreover, the enhanced protein-protein interaction between COX-2 and B55δ after AFB1 treatment was detected by immunoprecipitation (IP) assay (Fig. 6e), indicating that COX-2 might be dephosphorylated by PP2A-B55δ. To further investigate whether the phosphorylated status of COX-2 and its downstream functions could be regulated by B55δ, we established a knockdown model with si*PPP2R2D*. Compared to AFB1-treated siNC cells, the protein levels of B55δ, COX-2, and proteins representing assembly (NLRP3, ASC, and p10) and activation (IL-1β and GSDMD) of NLRP3 inflammasome were decreased (Fig. 6f). The fluorescence intensity of B55δ and co-localization between NLRP3 and mitochondria was inhibited in AFB1-treated si*PPP2R2D* cells (Fig. 6g), which consistent with reduced LDH leakage and IL-1β release with B55δ intervention (Fig. 6h, i), indicating that B55δ dephosphorylated COX-2 mediated NLRP3 inflammasome activation and pyroptosis-related plasma membrane rupture. These results suggest that dephosphorylated COX-2^{Ser601}, mediated by PP2A-B55δ, regulated its function for NLRP3 inflammasome activation.

Phosphorylation status of COX-2^{Ser601} determined its ER localization and degradation

Studies have revealed that N-glycosylated COX-2 at asparagine 594 determined its subcellular localization and 19 amino acids at C-terminal (Asn594-Lys612) were important for its degradation (Mbonye and Song 2009; Yuan and Smith 2015). In the present study, compared to COX-2^{S601A} cells, co-localization of COX-2 and ER-Tracker was stronger in COX-2^{S601D} cells detected by IF assay, indicating that phosphorylated COX-2^{Ser601} tends to remain in ER (Fig. 7a). The study has shown that Derlin 1, an ER-associated degradation (ERAD) core protein, could interact with COX-2 at C-terminal for cytosolic proteasome degradation (Chen et al. 2013; Mbonye et al. 2008). Compared to COX-2^{S601A} cells, the protein-protein interaction between COX-2 and Derlin 1 was increased in COX-2^{S601D} cells as detected by IP assay, while the interaction between COX-2 and B55δ was decreased (Fig. 7b). Meanwhile, compared to un-treated siNC cells, the protein-protein interaction and fluorescent co-localization between COX-2 and Derlin 1 were reduced, as analyzed by IP and IF assay, respectively (Fig. 7c, d), indicating that AFB1 inhibited the ERAD process of COX-2 via blocking COX-2-Derlin 1 interaction. Furthermore, compared to AFB1-treated siNC cells, the COX-2-Derlin 1 interaction was enhanced with B55δ intervention (Fig. 7c, d), indicating that PP2A-B55δ induced by AFB1 regulated ERAD of COX-2 via dephosphorylation of COX-2^{Ser601}. These data suggest that dephosphorylated modification of COX-2^{Ser601} by PP2A-B55δ determined its ER retention for proteasome degradation.

Discussion

We applied a COX-2 upregulation model with AFB1 to investigate the role of COX-2 in hepatic microenvironment during liver inflammatory progress. An upregulated hepatic mRNA level of *Ptgs2*, increased inflammatory infiltration, and an especially increased number of KCs were observed in vivo. CELE, a selective inhibitor of COX-2, relieved the inflammatory infiltration induced by AFB1, indicating that COX-2 may function as a potential molecular target for liver inflammatory injury. In the existing studies, COX-2 is proposed to have protective roles in multiple processes such as

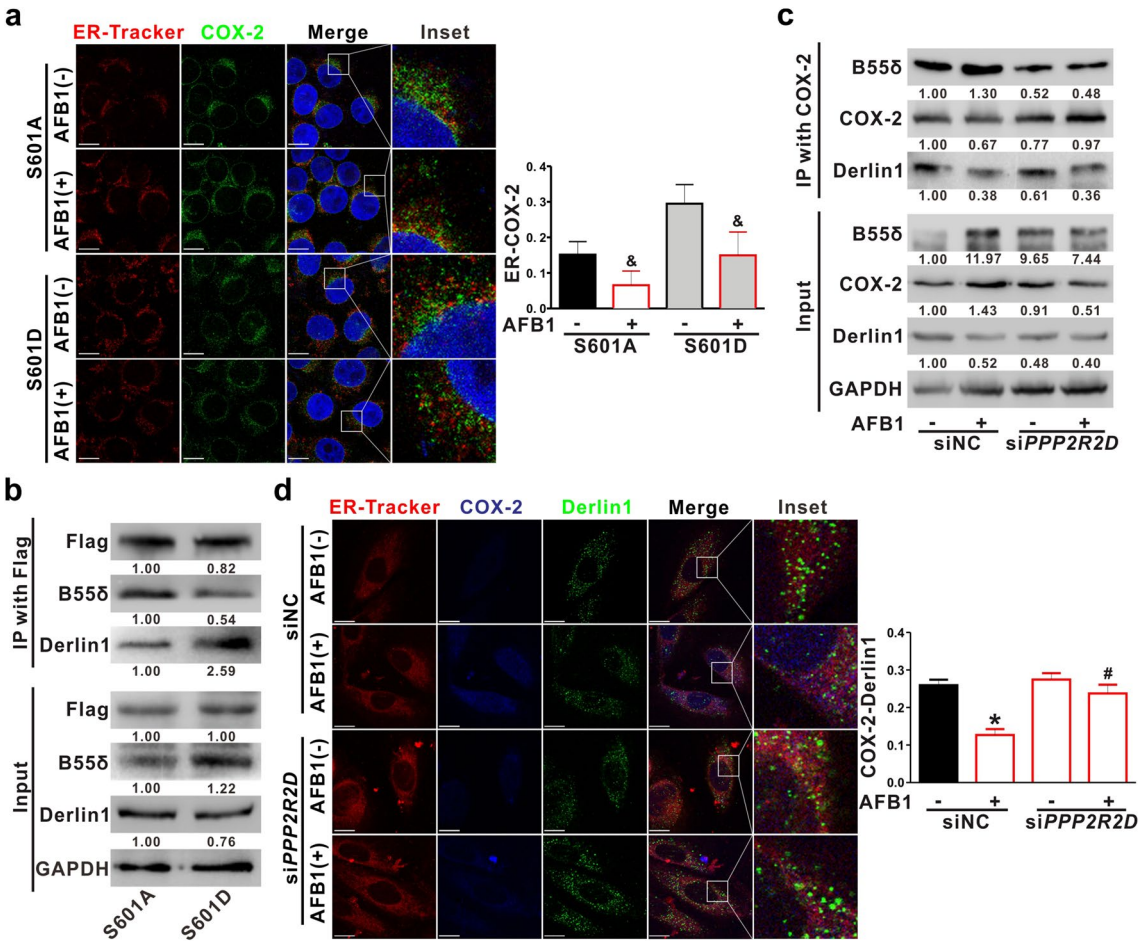

Fig. 7 Phosphorylation status of COX-2^{Ser601} determined its ER localization and degradation. **a** After treatment of AFB1 (1 μM, 24 h), the expression of COX-2 (green) in COX-2^{S601A} and COX-2^{S601D} cells was examined by confocal microscopy (left panel) ER-Tracker staining (red) represented the ER, and DAPI staining (blue) represented the nucleus. Scale bar 10 μm. Pearson's correlation for the co-localization of ER and COX-2 was shown in the bar graph (right panel). The overlap sections of ER and COX-2 were quantified using ImagePro-plus 6.0. **b** Cell lysates of COX-2^{S601A} and COX-2^{S601D} were immunoprecipitated with anti-Flag antibody, and both IP and total lysates (Input) were immunoblotted for Flag, B55δ, and Derlin 1. **c**, **d** Differentiated HepaRG cells were transfected with siNC or si*PPP2R2D* (50 nM) for 6 h, followed by AFB1 treatment (1 μM, 24 h). Cell lysates were immunoprecipitated with anti-COX-2 antibody, and both IP and Input were immunoblotted with B55δ, COX-2, and Derlin 1 (**c**). The expression of Derlin 1 (green) and COX-2 (blue), and co-localization with ER (red) was examined by confocal microscopy (left panel). Scale bar 10 μm. Pearson's correlation for the co-localization of COX-2 with Derlin 1 was shown in the bar graph (right panel). The overlap sections of COX-2 and Derlin 1 were quantified using ImagePro-plus 6.0 (**d**). GAPDH served as a loading control for WB analysis. Representative examples were displayed. All data were shown as mean ± SD. $^{*}P < 0.05$, compared with siNC control group. $^{\#}P < 0.05$, compared with siNC and AFB1-treated group. $^{\&}P < 0.05$, compared with untreated group (colour figure online)

oxidative stress, liver inflammation, and fibrosis in hepatocyte-specific COX-2 transgenic (hCOX-2-Tg) mice; however, the pro-inflammatory role of COX-2 remain a focus (Motino et al. 2016, 2019). In different models, hepatic metabolic enzymes may influence oxidative stress and inflammatory mediators (Cobbina and Akhlaghi 2017). In our study with AFB1-treated mice model, *Cyp1a2* and *Cyp3a11* of hepatic CYPs, phase I drug-metabolizing enzymes for metabolism were upregulated, while *Gsta*, *Gstm*, *Gstt* of GSTs, phase II drug-metabolizing enzymes for detoxification were down-regulated. In the current in vitro studies, we used HepaRG cells and primary hepatocytes because they are metabolically competent to solve the loss of metabolic capacity in immortalized cells lines (Bell et al. 2017; Yuan et al. 2018).

Consistent with a report demonstrating that AFB1 formed a hepatic pro-inflammatory microenvironment in zebrafish via transcriptional activity of NF-κB, promoting expression of COX-2 and IL-6 (Lu et al. 2013), our study showed that hepatic mRNA level of pro-inflammatory cytokines, *Ptgs2*, *Il1b*, *Il18*, *Il6*, and *Tnfa* were significantly increased after AFB1 treatment. Due to the ability of KCs for secreting various cytokines, we supposed a KCs-hepatocytes

feedback loop to promote liver inflammatory injury. In the present study, DAMPs and IL-1β released from pyroptotic hepatocytes activated F4/80 positive KCs (M1 phenotype) to secrete pro-inflammatory cytokines in an NLRP3-dependent and transcriptional way, forming an immune microenvironment to amplify liver inflammatory injury. Our results are in agreement with a report by Wree et al., that overexpression of NLRP3 in global and myeloid-specific *Nlrp3* knock-in mice contributed to pyroptosis of hepatocytes and leukocytes, resulting in severe liver inflammation (Wree et al. 2014). For transcriptional factors, studies have revealed that c-Jun NH2-terminal kinases (JNKs), a major kinase to phosphorylate c-Jun, activated by a wide range of stimulus, played an important role in obesity-induced liver inflammation and steatosis, especially in adipose and liver tissue (Pal et al. 2016). Active c-Jun, as a component of transcription factor AP-1, promoted the expression of pro-inflammatory cytokines, such as TNF-α, IL-6, and IL-1β. Moreover, IL-6, derived from KCs, influenced phosphorylation of STAT3 to translocate to the nucleus for pro-inflammatory signaling. Knockout of hepatic STAT3 prevented HSC activation and hepatic fibrosis by decreasing the release of fibrogenic cytokines (Deng et al. 2013). The activation of STAT3 signaling pathway mediated the pro-inflammatory immune cascades, which promoted the formation of hepatic immune microenvironment and liver inflammatory injury. Consistent with our data, slight collagen deposition was observed in parallel with NLRP3 inflammasome activation in liver tissues. Studies have demonstrated the direct role of NLRP3 inflammasome to trigger liver inflammation and fibrosis through HSC activation in *Nlrp3*$^{-/-}$ mice (Inzaugarat et al. 2019; Mridha et al. 2017). In the current study, pro-inflammatory signaling of KCs formed a regional immune microenvironment to aggravate NLRP3 inflammasome activation in AFB1-exposed hepatocytes.

Moreover, in hepatocytes, dephosphorylated COX-2^{Ser601} promoted mitochondrial translocation of NLRP3, facilitating assembly of NLRP3 inflammasome with its adaptor protein ASC at the mitochondria, resulting in IL-1β release and pyroptosis. In response to pathogens or DAMPs, NLRP3 inflammasome experiences two steps to induce caspase 1-dependent pyroptosis: first, transcriptionally encoded NLRP3, pro-IL-1β, and pro-IL-18 are released into the cytosol via NF-κB pathway; then, they are translocated to mitochondria to form a platform of caspase 1 with ASC when stimulus, such as disorder of ER reduction-oxidation (ER-redox), unfolded protein response (UPR), mitochondrial damage, and cathepsin, occurs (Rathinam and Fitzgerald 2016; Rubartelli 2012). ER-redox homeostasis, determined by its signaling mediators endoplasmic reticulum reductive protein 1α (ERO1α) and protein disulfide isomerase (PDI), plays a vital role as the trigger and an effector to UPR (Zeeshan et al. 2016). In our study, AFB1 induced COX-2 upregulation and NLRP3 inflammasome activation via the modulation of ERO1α-dependent ER redox homeostasis mediated by ER response (including ATF4-associated ER stress) pathway. There was the ATF4-ERO1α-COX-2-NLRP3 axis as one of the direct evidences to state that AFB1 induced NLRP3 inflammasome-dependent pyroptosis via upregulated COX-2 in hepatocytes (unpublished data).

While previous studies suggested that COX-2 or PGs activated NLRP3 inflammasome via mitochondrial dysfunctions in macrophages (Hua et al. 2015; Liu et al. 2018), our data reveal that COX-2 interacted with NLRP3 at mitochondria and co-regulated NLRP3 inflammasome assembly and activation. As shown in our previous study, mitochondrial translocation of COX-2 promoted the cancer stemness of nasopharyngeal carcinoma via recruiting mitochondrial p53 and Drp1 for fission (Zhou et al. 2017). Here, we propose that dephosphorylated COX-2, which is synthesized and modified in ER, as a mediator between ER disturbance and mitochondrial dysfunction, mediating assembly and activation of NLRP3 inflammasome. As for ER-mitochondria crosstalk of NLRP3, Zhang et al. proposed that increased thioredoxin interaction protein (TXNIP), which stimulated by reduction-oxidation (redox) disturbance, promoted inflammation and lipid accumulation via activating the NLRP3 inflammasome in fructose-mediated NASH model (Zhang et al. 2015). Bronner et al. revealed that IRE1, a sensor of unfolded protein response in ER, mediated cleavage activity of caspase 2, which facilitated NLRP3 inflammasome activation through releasing mitochondrial contents from bone-marrow-derived macrophages (Bronner et al. 2015). Moreover, NLRP3 can be recruited on mitochondria-associated ER membranes (MAM) (Zhou et al. 2011). We have previously demonstrated that COX-2 could be located on MAM and regulated Ca^{2+} transport and mitochondrial-associated apoptosis. Whether COX-2 interacts with NLRP3 on MAM and co-transfers to mitochondria through MAM remains to be further explored.

ER is a focal point of PQC because of the complicated folding, modification, and degradation process (Buchberger 2014). In response to xenobiotics, misfolded or unfolded protein is accumulated in the ER lumen. To maintain ER homeostasis, ERAD, one of the quality control mechanisms, is activated to eliminate accumulated proteins for cellular adaption (Sun and Brodsky 2017). Moreover, phosphorylation or dephosphorylation, a type of post-translational modification, plays an important role in the subcellular distribution, functional activity, and degradation of proteins (Klement and Medzihradszky 2017). Therefore, the mechanism of COX-2 for its phosphorylation and degradation is of interest to study. It has been studied that STEL (601–604, last 4 amino acid at C-terminal of COX-2), as an inefficient ER retention signal of COX-2, tends to transport to Golgi for PGs synthesis which slowed down retrograde movement

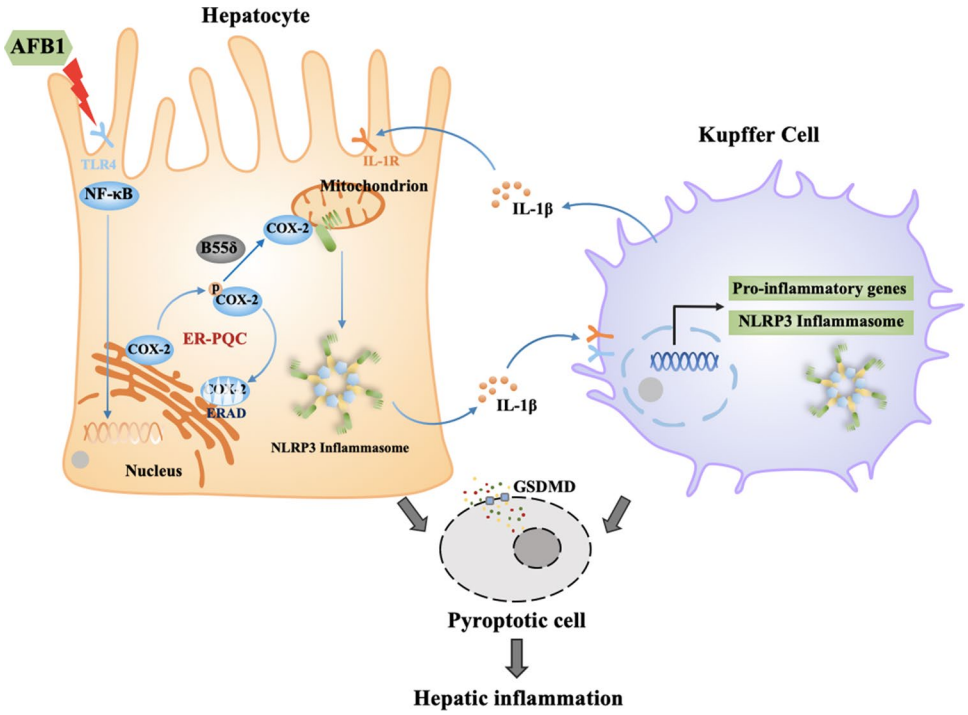

Fig. 8 AFB1 enhances pyroptosis of hepatocytes and activation of Kupffer cells to promote liver inflammatory injury via dephosphorylation of COX-2. Dephosphorylation of p-COX-2^{Ser601} by PP2A-B55δ induced by AFB1, altered its ER localization and ERAD, to promote its regulatory function on NLRP3 inflammasome activation in hepatocytes. Moreover, IL-1β and DAMPs released from pyroptotic hepatocytes stimulate pro-inflammatory signaling of KCs, to form regional immune response cascades which amplified NLRP3-dependent pyroptosis of hepatocytes and liver inflammation

back to ER for degradation (Yuan and Smith 2015). Replacement of STEL with KDEL (a mutation from serine-threonine to lysine-aspartate at 601–602), a potent ER retention signal of COX-2, like DTEL (a mutation from serine to aspartate at 601) of our study, could concentrate COX-2 in ER for degradation. In the current study, mimic phosphorylation and dephosphorylation of COX-2^{Ser601} were used to investigate the distribution and function of COX-2. For ERAD, Derlin 1 brought protein from ER to cytosolic through the retro-translocation channel, to enhance interaction between caveolin-1 (CAV-1) and COX-2 relying on its C-terminal for proteasome degradation (Chen et al. 2013; Mbonye et al. 2008). Our results are in agreement with these data that serine 601 at C-terminal of COX-2 determined its localization and degradation. Furthermore, for the first time, we proposed that COX-2 could be dephosphorylated by PP2A-B55δ. Phosphorylated COX-2^{Ser601} has the potential to concentrate in ER and interact with Derlin 1 for degradation after B55δ intervention, while dephosphorylated COX-2^{Ser601} by B55δ promoted NLRP3 inflammasome activation in hepatocytes.

In summary, our findings point out a novel dephosphorylation modification of p-COX-2^{Ser601} induced by AFB1 alters the ER localization of COX-2 and ERAD and therefore promotes its regulatory function on NLRP3 inflammasome activation in hepatocytes. Moreover, IL-1β and DAMPs released from pyroptotic hepatocytes stimulate STAT3-mediated pro-inflammatory signaling of KCs, to form regional immune response cascades which amplified NLRP3-dependent pyroptosis of hepatocytes and liver inflammation. COX-2 could be a potential target molecule for prevention and therapy of the inducible NLRP3 inflammasome and liver inflammatory injury (Fig. 8).

Acknowledgements We appreciate Prof. Xian-Ming Deng (Life Sciences School, Xiamen University, China) for his kind gift of CY-09. We appreciate Mr. Blake Xunbai Mei for English editing. This study was supported by grants from the National Natural Science Foundation of China (Nos. 81773465, 81973082, 81573181, and 81874272), Early-stage Project of National Key Basic Research Program of China (No. 2014CB560710), the Natural Science Foundation of Fujian Province of China (Nos. 2014J01372, 2015J01344), and the Scientific Research Foundation of State Key Laboratory of Molecular Vaccinology and Molecular Diagnostics (No. 2017ZY003).

Compliance with ethical standards

Conflict of interest All authors declare that they have no conflict of interest.

References

Akinrinmade FJ, Akinrinde AS, Amid A (2016) Changes in serum cytokine levels, hepatic and intestinal morphology in aflatoxin B1-induced injury: modulatory roles of melatonin and flavonoid-rich fractions from Chromolena odorata. Mycotoxin Res 32(2):53–60. https://doi.org/10.1007/s12550-016-0239-9

Alexanian A, Sorokin A (2017) Cyclooxygenase 2: protein-protein interactions and posttranslational modifications. Physiol Genom 49(11):667–681. https://doi.org/10.1152/physiolgenomics.00086.2017

Alvarez-Fernandez M, Sanz-Flores M, Sanz-Castillo B et al (2018) Therapeutic relevance of the PP2A-B55 inhibitory kinase MASTL/Greatwall in breast cancer. Cell Death Differ 25(5):828–840. https://doi.org/10.1038/s41418-017-0024-0

Bell CC, Lauschke VM, Vorrink SU et al (2017) Transcriptional, functional, and mechanistic comparisons of stem cell-derived hepatocytes, HepaRG Cells, and three-dimensional human hepatocyte spheroids as predictive in vitro systems for drug-induced liver injury. Drug Metab Dispos 45(4):419–429. https://doi.org/10.1124/dmd.116.074369

Bertran MT, Mouilleron S, Zhou Y et al (2019) ASPP proteins discriminate between PP1 catalytic subunits through their SH3 domain and the PP1 C-tail. Nat Commun 10(1):771. https://doi.org/10.1038/s41467-019-08686-0

Bronner DN, Abuaita BH, Chen X et al (2015) Endoplasmic reticulum stress activates the inflammasome via NLRP3- and caspase-2-driven mitochondrial damage. Immunity 43(3):451–462. https://doi.org/10.1016/j.immuni.2015.08.008

Buchberger A (2014) ERQC autophagy: yet another way to die. Mol Cell 54(1):3–4. https://doi.org/10.1016/j.molcel.2014.03.037

Byun JS, Yi HS (2017) Hepatic immune microenvironment in alcoholic and nonalcoholic liver disease. Biomed Res Int 2017:6862439. https://doi.org/10.1155/2017/6862439

Chen SF, Wu CH, Lee YM et al (2013) Caveolin-1 interacts with Derlin-1 and promotes ubiquitination and degradation of cyclooxygenase-2 via collaboration with p97 complex. J Biol Chem 288(46):33462–33469. https://doi.org/10.1074/jbc.M113.521799

Cobbina E, Akhlaghi F (2017) Non-alcoholic fatty liver disease (NAFLD)—pathogenesis, classification, and effect on drug metabolizing enzymes and transporters. Drug Metab Rev 49(2):197–211. https://doi.org/10.1080/03602532.2017.1293683

Deng YR, Ma HD, Tsuneyama K et al (2013) STAT3-mediated attenuation of CCl4-induced mouse liver fibrosis by the protein kinase inhibitor sorafenib. J Autoimmun 46:25–34. https://doi.org/10.1016/j.jaut.2013.07.008

Garg AD, Galluzzi L, Apetoh L et al (2015) Molecular and translational classifications of DAMPs in immunogenic cell death. Front Immunol 6:588. https://doi.org/10.3389/fimmu.2015.00588

He C, Qiu Y, Han P et al (2018) ER stress regulating protein phosphatase 2A-B56gamma, targeted by hepatitis B virus X protein, induces cell cycle arrest and apoptosis of hepatocytes. Cell Death Dis 9(7):762. https://doi.org/10.1038/s41419-018-0787-3

Hua KF, Chou JC, Ka SM et al (2015) Cyclooxygenase-2 regulates NLRP3 inflammasome-derived IL-1beta production. J Cell Physiol 230(4):863–874. https://doi.org/10.1002/jcp.24815

Inzaugarat ME, Johnson CD, Holtmann TM et al (2019) NLR family pyrin domain-containing 3 inflammasome activation in hepatic stellate cells induces liver fibrosis in mice. Hepatology 69(2):845–859. https://doi.org/10.1002/hep.30252

Jiang H, He H, Chen Y et al (2017) Identification of a selective and direct NLRP3 inhibitor to treat inflammatory disorders. J Exp Med 214(11):3219–3238. https://doi.org/10.1084/jem.20171419

Julien O, Wells JA (2017) Caspases and their substrates. Cell Death Differ 24(8):1380–1389. https://doi.org/10.1038/cdd.2017.44

Klement E, Medzihradszky KF (2017) Extracellular protein phosphorylation, the neglected side of the modification. Mol Cell Proteom 16(1):1–7. https://doi.org/10.1074/mcp.O116.064188

Koyama Y, Brenner DA (2017) Liver inflammation and fibrosis. J Clin Invest 127(1):55–64. https://doi.org/10.1172/jci88881

Lamkanfi M, Dixit VM (2014) Mechanisms and functions of inflammasomes. Cell 157(5):1013–1022. https://doi.org/10.1016/j.cell.2014.04.007

Li WC, Ralphs KL, Tosh D (2010) Isolation and culture of adult mouse hepatocytes. Methods Mol Biol 633:185–196. https://doi.org/10.1007/978-1-59745-019-5_13

Li P, He K, Li J, Liu Z, Gong J (2017) The role of Kupffer cells in hepatic diseases. Mol Immunol 85:222–229. https://doi.org/10.1016/j.molimm.2017.02.018

Liao K, Xia B, Zhuang QY et al (2015) Parthenolide inhibits cancer stem-like side population of nasopharyngeal carcinoma cells via suppression of the NF-kappaB/COX-2 pathway. Theranostics 5(3):302–321. https://doi.org/10.7150/thno.8387

Liu Y, Duan C, Chen H et al (2018) Inhibition of COX-2/mPGES-1 and 5-LOX in macrophages by leonurine ameliorates monosodium urate crystal-induced inflammation. Toxicol Appl Pharmacol 351:1–11. https://doi.org/10.1016/j.taap.2018.05.010

Lu JW, Yang WY, Lin YM et al (2013) Hepatitis B virus X antigen and aflatoxin B1 synergistically cause hepatitis, steatosis and liver hyperplasia in transgenic zebrafish. Acta Histochem 115(7):728–739. https://doi.org/10.1016/j.acthis.2013.02.012

Mbonye UR, Song I (2009) Posttranscriptional and posttranslational determinants of cyclooxygenase expression. BMB Rep 42(9):552–560. https://doi.org/10.5483/bmbrep.2009.42.9.552

Mbonye UR, Yuan C, Harris CE et al (2008) Two distinct pathways for cyclooxygenase-2 protein degradation. J Biol Chem 283(13):8611–8623. https://doi.org/10.1074/jbc.M710137200

Mokdad AA, Lopez AD, Shahraz S et al (2014) Liver cirrhosis mortality in 187 countries between 1980 and 2010: a systematic analysis. BMC Med 12:145. https://doi.org/10.1186/s12916-014-0145-y

Motino O, Agra N, Brea Contreras R et al (2016) Cyclooxygenase-2 expression in hepatocytes attenuates non-alcoholic steatohepatitis and liver fibrosis in mice. Biochim Biophys Acta 1862(9):1710–1723. https://doi.org/10.1016/j.bbadis.2016.06.009

Motino O, Frances DE, Casanova N et al (2019) Protective role of hepatocyte cyclooxygenase-2 expression against liver ischemia-reperfusion injury in mice. Hepatology 70(2):650–665. https://doi.org/10.1002/hep.30241

Mridha AR, Wree A, Robertson AAB et al (2017) NLRP3 inflammasome blockade reduces liver inflammation and fibrosis in experimental NASH in mice. J Hepatol 66(5):1037–1046. https://doi.org/10.1016/j.jhep.2017.01.022

Pal M, Febbraio MA, Lancaster GI (2016) The roles of c-Jun NH2-terminal kinases (JNKs) in obesity and insulin resistance. J Physiol 594(2):267–279. https://doi.org/10.1113/jp271457

Rathinam VA, Fitzgerald KA (2016) Inflammasome complexes: emerging mechanisms and effector functions. Cell 165(4):792–800. https://doi.org/10.1016/j.cell.2016.03.046

Reynhout S, Janssens V (2018) Physiologic functions of PP2A: lessons from genetically modified mice. Biochim Biophys Acta Mol Cell Res 1866(1):31–50. https://doi.org/10.1016/j.bbamcr.2018.07.010

Rubartelli A (2012) Redox control of NLRP3 inflammasome activation in health and disease. J Leukoc Biol 92(5):951–958. https://doi.org/10.1189/jlb.0512265

Rushing BR, Selim MI (2019) Aflatoxin B1: a review on metabolism, toxicity, occurrence in food, occupational exposure, and detoxification methods. Food Chem Toxicol 124:81–100. https://doi.org/10.1016/j.fct.2018.11.047

Sarhan M, Land WG, Tonnus W, Hugo CP, Linkermann A (2018) Origin and consequences of necroinflammation. Physiol Rev 98(2):727–780. https://doi.org/10.1152/physrev.00041.2016

Sun Z, Brodsky JL (2017) Guardians of the ERAD Galaxy. Cell 171(2):267–268. https://doi.org/10.1016/j.cell.2017.09.023

Ueng YF, Shimada T, Yamazaki H, Guengerich FP (1995) Oxidation of aflatoxin B1 by bacterial recombinant human cytochrome P450 enzymes. Chem Res Toxicol 8(2):218–225

Van Opdenbosch N, Lamkanfi M (2019) Caspases in cell death, inflammation, and disease. Immunity 50(6):1352–1364. https://doi.org/10.1016/j.immuni.2019.05.020

Virshup DM, Shenolikar S (2009) From promiscuity to precision: protein phosphatases get a makeover. Mol Cell 33(5):537–545. https://doi.org/10.1016/j.molcel.2009.02.015

Wree A, Eguchi A, McGeough MD et al (2014) NLRP3 inflammasome activation results in hepatocyte pyroptosis, liver inflammation, and fibrosis in mice. Hepatology 59(3):898–910. https://doi.org/10.1002/hep.26592

Yuan C, Smith WL (2015) A cyclooxygenase-2-dependent prostaglandin E2 biosynthetic system in the Golgi apparatus. J Biol Chem 290(9):5606–5620. https://doi.org/10.1074/jbc.M114.632463

Yuan L, Liu X, Zhang L et al (2018) Optimized HepaRG is a suitable cell source to generate the human liver chimeric mouse model for the chronic hepatitis B virus infection. Emerg Microbes Infect 7(1):144. https://doi.org/10.1038/s41426-018-0143-9

Zeeshan HM, Lee GH, Kim HR, Chae HJ (2016) Endoplasmic reticulum stress and associated ROS. Int J Mol Sci 17(3):327. https://doi.org/10.3390/ijms17030327

Zhang X, Zhang JH, Chen XY et al (2015) Reactive oxygen species-induced TXNIP drives fructose-mediated hepatic inflammation and lipid accumulation through NLRP3 inflammasome activation. Antioxid Redox Signal 22(10):848–870. https://doi.org/10.1089/ars.2014.5868

Zhang Y, Chen X, Gueydan C, Han J (2018) Plasma membrane changes during programmed cell deaths. Cell Res 28(1):9–21. https://doi.org/10.1038/cr.2017.133

Zhou R, Yazdi AS, Menu P, Tschopp J (2011) A role for mitochondria in NLRP3 inflammasome activation. Nature 469(7329):221–225. https://doi.org/10.1038/nature09663

Zhou TJ, Zhang SL, He CY et al (2017) Downregulation of mitochondrial cyclooxygenase-2 inhibits the stemness of nasopharyngeal carcinoma by decreasing the activity of dynamin-related protein 1. Theranostics 7(5):1389–1406. https://doi.org/10.7150/thno.17647